Joining of cemented carbides to steel by laser beam welding

Laserstrahlschweißen von Stahl-Hartmetall/Cermet-Verbindungen

C. Barbatti[1], J. Garcia[1], G. Liedl[2], A. Pyzalla[1]

Welding of dissimilar materials such as steel and cemented carbides (hardmetals, cermets) is particularly challenging e.g. because mismatches in their thermal expansion coefficients and thermal conductivities result in residual stress formation and because of the formation of brittle intermetallic phases. Laser beam welding of cemented carbides to steel appears as an attractive complementary technique to conventional brazing processes due to its high precision, high process speed, low heat input and the option of welding without filler.

Here a laser welding process including pre-heat treatment and post-heat treatment was applied successfully to joining as-sintered and nitrided hardmetals and cermets to low alloyed steel. The microstructure and mechanical properties of the welds are investigated by microscopy, X-ray diffraction, microhardness measurements, and bending tests. The results reveal that the three-step laser beam welding process produced crack-free and non-porous joints. Nitridation of the cemented carbides results in a significant reduction of the amount of brittle intermetallic phases. The mechanical properties of the joints are competitive to those of the conventional brazed steel-cemented carbide joints.

Keywords: hardmetals; cermets; nitridation; laser beam welding; η-phases.

Das Schweißen von ungleichartigen Werkstoffen wie z. B. Stählen mit Hartmetallen und Cermets stellt eine erhebliche Herausforderung dar, u. a. infolge der unterschiedlichen thermischen Ausdehnungskoeffizienten und Wärmeleitfähigkeiten, welche die Bildung von Eigenspannungen zur Folge haben, sowie aufgrund der Bildung spröder intermetallischer Phasen. Das Laserstrahlschweißen von Hartmetallen/Cermets mit Stahl erscheint als attraktives komplementäres Verfahren zum üblicherweise verwendeten Löten, da es die Herstellung von Verbindungen mit höherer Präzision, höherer Geschwindigkeit sowie geringerem Wärmeeintrag erlaubt und die Verwendung eines Zusatzwerkstoffs nicht notwendig ist.

Gesinterte und nitrierte Hartmetalle/Cermets wurden mit einem Vergütungsstahl durch einen dreistufigen Laserstrahlschweißprozess, der eine Vor- und Nachwärmebehandlung enthält, verbunden. Das Gefüge und die mechanischen Eigenschaften der Verbindung wurden mittels Mikroskopie, Röntgendiffraktion, Mikrohärtemessungen und Biegeversuchen charakterisiert. Die Ergebnisse zeigen, dass mit dem dreistufigen Laserstrahlschweißprozess riss- und porenfreie Verbindungen hergestellt werden konnten. Das Nitrieren der Hartmetalle/Cermets führte zu einer deutlichen Verringerung der Bildung spröder intermetallischer Phasen. Die mechanischen Eigenschaften der Stahl - Hartmetall/Cermet – Verbindungen sind vergleichbar mit den Eigenschaften entsprechender gelöteter Verbindungen.

Schlüsselworte: Hartmetalle; Cermets; Nitrieren; Laserstrahlschweißen; η-Phasen.

1 Introduction

Cemented carbides are multiphase materials comprising a hard phase skeleton composed of refractory metal carbides e.g. WC, TiC embedded in a metallic binder (Co, Ni, Fe). Cemented carbides are manufactured by liquid phase sintering of compacted mixtures of carbide and binder metal powders.

Due to their high hardness and superior wear resistance, cemented carbides are used as tools for cutting, milling, and machining. They are optimized for these different applications by varying the binder content as well as the composition and grain size of the hard phases [1,2]. Because cemented carbides are brittle and expensive materials, it can be favourable to join them to steel substrates, e.g. in case of saw blades for wood machining applications, where cemented carbides are used as saw tooth tips.

Cemented carbides today are most often joined to steel by mechanical clamping [3], brazing [4] or resistance welding [5]. Other welding methods are rarely used because of the challenges arising e.g. from thermal expansion coefficient and thermal conductivity mismatch between steel and cemented carbide. In addition, at the cemented carbide/steel interface diffusion of C from the cemented carbides into the steel [6] may result in the formation of brittle η-phases (ternary mixed carbide phases, e.g. M_6C and $M_{12}C$). Both the thermal expansion and conductivity mismatch and the formation of brittle η-phases may result in porosity and crack formation in cemented carbide/steel joints; see for instance [7].

Laser beam welding of cemented carbides to steels compared to other welding processes might be advantageous due to its focussed heat input, high precision and high process speed [8–11]. So far, however, exclusively joints between cemented carbides with WC concentrations above 88 wt.-% WC and without mixed carbide additions (*Figure 1*) were studied [7–11].

The aim of this study is a first spot check on the possibility of joining steel to hardmetals with a wider range of WC and mixed carbide contents. In addition, an attempt at controlling η-phase formation by nitridation of the cemented carbides is made. In contrast to the investigations cited above, here a three-step laser welding process is employed [12]. This three-step welding process includes pre-heating, welding, and post-heating in order to minimize temperature gradients

[1] Max-Planck-Institut für Eisenforschung GmbH , 40237 Düsseldorf, Germany

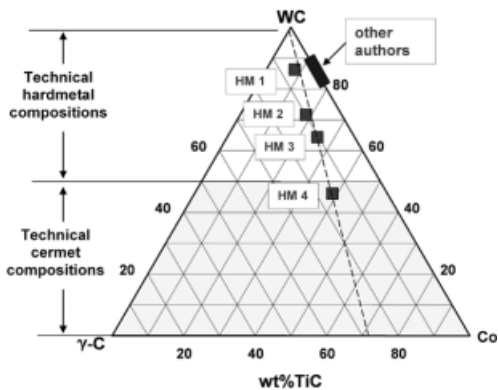[2] TU Wien, Institut für Umform- und Hochleistungslasertechnik (IFLT), 1040 Vienna, Austria

Figure 1. Samples investigated in the WC-γC-Co system, γC=(Ti,Ta,Nb)C.
Bild 1. Zusammensetzung der untersuchten Proben im System WC- γC-Co, γC=(Ti,Ta,Nb)C.

Table 1. Chemical composition of the cemented carbides investigated.
Tabelle 1. Zusammensetzung der untersuchten Proben.

Material	Chemical Composition [wt%]		
	WC	γ-Phase	Co
HM1	85	9	6
HM2	70	20	10
HM3	65	25	10
HM4	43	42	15

and avoid crack formation in the cemented carbide / steel joints. Several laser beam welding conditions (e.g. laser power, time) as well as different weld geometries are studied.

2 Experimental

2.1 Materials

Four cemented carbide compositions were selected, which cover a wide range of technical applications according to ISO 513:2004. The main difference in the composition of the alloys investigated is their WC content varying between typical values of hardmetals (85wt.-% WC) to typical cermet compositions (45wt.-% WC) [1], Figure 1. For the sake of briefness, we present only three of the welded samples in detail, comparing e.g. a hardmetal/steel to a nitrided hardmetal/steel weld as well as hardmetal/steel and cermet/steel welds.

Green compacts with dimensions $5\,mm \times 5\,mm \times 1\,mm$ ($l \times w \times t$) were produced on a laboratory scale by powder sintering techniques (*Table 1*). The Co binder and hard phase (W,Ti)C, WC, (Ta,Nb)C powders were mixed, pressed, and fully densified via liquid phase sintering. The samples were sintered in vacuum at $1450\,°C$. The hardmetal (HM3) and the cermet (HM4) were heat treated at $1350\,°C$ under nitrogen-rich atmosphere. The cemented carbides were welded to low alloyed hypoeutectoid steel (1.1231: 0.72%C, 0.2%Si, 0.55%Mn, 0.03%P, 0.02%S).

Table 2. Main process parameters of the laser beam welding process.
Tabelle 2. Parameter des dreistufigen Laserstrahlschweißprozess

	Pre-heating	Welding	Post-heating
Laser Power (kW)	0.2–0.3	0.6–1.0	0.2
Time (s)	1.5	2.0	0.5–1.0
f.p.p. (mm)	0	0	0
Shielding gas (lmin)	10	10	10

2.2 Laser beam welding

A Nd:YAG laser source (1995 model Raster Zeulenroda semiconductor diode laser) in continuous wave mode operating with a maximum output power of 1.0 kW was used to join the cemented carbide parts to a steel holder. To ensure sufficient degree of contact, the workpieces were clamped face to face in a butt-weld configuration**.** Oxidation was prevented by using argon shielding gas (10 l/min). The laser beam spot was positioned 2/3 onto the cemented carbide and 1/3 onto the steel; the vertical point position was 0 mm. The welding process consisted of pre-heating, welding, and post-weld heat treatment (*Table 2*).

2.3 Metallography and Microscopy

Samples for optical microscopy and scanning electron microscopy (SEM) analyses were prepared by cutting cross-sections perpendicular to the direction of the laser beam motion, followed by grinding and polishing with diamond suspension down to 3 µm. SEM was performed using a Schottky field emission gun JEOL JSM 6500F equipped with an energy dispersive (EDX) analysis system. Microstructure analyses (phase, grain size) in the fusion zone and steel base material were obtained by automated indexing of electron backscattering diffraction (EBSD) patterns. The measurements were carried out in the SEM using an EDAX/TSL EBSD system equipped with a Digitview camera.

Vickers microhardness ($HV_{0.05}$) profiles on the weld cross-section and the base materials were performed on polished samples.

2.4 X-ray diffraction

In order to assess the phase constitution after laser beam welding, X-ray diffraction (XRD) measurements were performed in the fusion zone of the cemented carbide/steel joints. Residual stress distributions in longitudinal and transverse direction were determined across the weld from the steel towards the cemented carbide side. Residual stress measurements by the $\sin^2\psi$-method [13] were performed using synchrotron radiation at the experimental station G3 at DORIS III at HASYLAB at DESY, Hamburg. The radiation energy was 6.9keV (λ_{Co}=1.7904 nm), area of incidence 1 mm×1 mm, mm, ψ range $0\,°$ to $63\,°$, step size ± 0.2 in $\sin^2\psi$. The Fe (211) reflection and the WC (201) reflection were chosen in the steel and the cemented carbide, respectively.

2.5 Bending tests

Bending tests were performed with a maximum load of 10 kN and a deformation rate of 0.5 mm/min with a similar procedure as in [11]. The steel side of the specimen was clamped and load was applied at the centre of the cemented carbide part.

3 Results

3.1 Microstructure of the base materials

3.1.1 Hardmetals

Microstructure in the as-sintered state: In the typical microstructure of the as-sintered hardmetal, WC particles appear as white faceted single crystals, while the γ-phase (Ti,Ta,Nb)C has a spherical morphology (*Figure 2a).* The average size of the WC is about 1.5 μm, although several grains can be as large as 4 μm, showing a rectangular morphology instead of the usual prismatic one. The γ-phase grains usually do not exceed 2 μm grain size. The Co binder appears as a dark grey network surrounding the homogeneously distributed hard phases (Figure 2a).

Microstructure after nitridation: A post-sintering heat treatment in nitrogen-containing atmosphere results in the formation of a 10 μm thick surface layer enriched in Ti(C,N) further referred to as γN-phase. The γN-phase layer is characterized by the absence of WC grains and the lower amount of Co in comparison to the bulk. [14, 15].

3.1.2 Cermets

Microstructure in the as-sintered state: The microstructure of the as-sintered cermet is also characterized by a homogeneous distribution of hard phases embedded in the metallic matrix (*Figure 2b).* SEM/BSE imaging and EDX analysis reveal the core-rim structure (Ti rich core, W and Ta rich rim) of the γ-phase typical for cermets [16]. EBSD analysis also reveals different crystalline orientations associated with the core and rim within the same γ-phase grain, implying the existence of a polycrystalline structure. The Co binder appears as the dark-gray network-like structure surrounding the hard phases. The average size of the γ-phase does not exceed 2 μm whereas the WC phases can reach 4 μm.

Microstructure after nitridation: Nitridation of the cermet results in a thicker 20 μm surface layer of γN-phase. The γN-phase has the same spherical morphology and size distribution and core-rim structure as the γ-phase in the bulk.

3.1.3 Steel

The microstructure of the steel is composed of ferrite and mainly pearlite with an average grain size of 2.8 μm.

3.2 Microstructure of the welded joints

A main characteristic of the laser beam welded cemented carbide/steel joints are their narrow, homogeneous weld beads (*Figure 3).* In case of high heat input occasionally steel melt can be 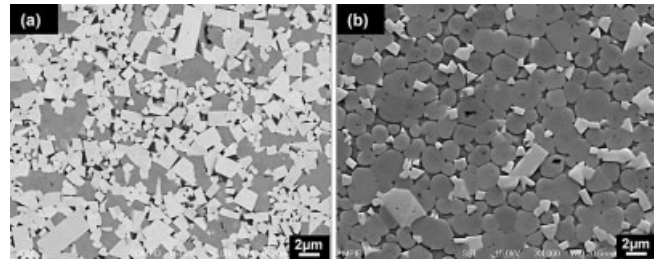observed on top of the cemented carbide. The fusion zone extends deeper into the steel part than into the cemented carbides. The heat affected zone in the steel part is substantially larger than in cemented carbide part. In all joints neither cracks nor pores were observed in the fusion zone. However cracks appeared at the transition between the heat affected zone and cemented carbide base material in joints with different thickness of cemented carbide and steel parts as well as in joints where the thickness of the cemented carbide or the steel part exceeded 1.5 mm.

3.2.1 Steel to Hardmetal Welds

A macroscopic view onto the cross-section of the joints reveals the fusion zone and heat affected zones (HAZ) that can be as wide as 1 mm in the steel (containing martensite) and a narrow heat affected zone about 100 μm wide in the hardmetal.
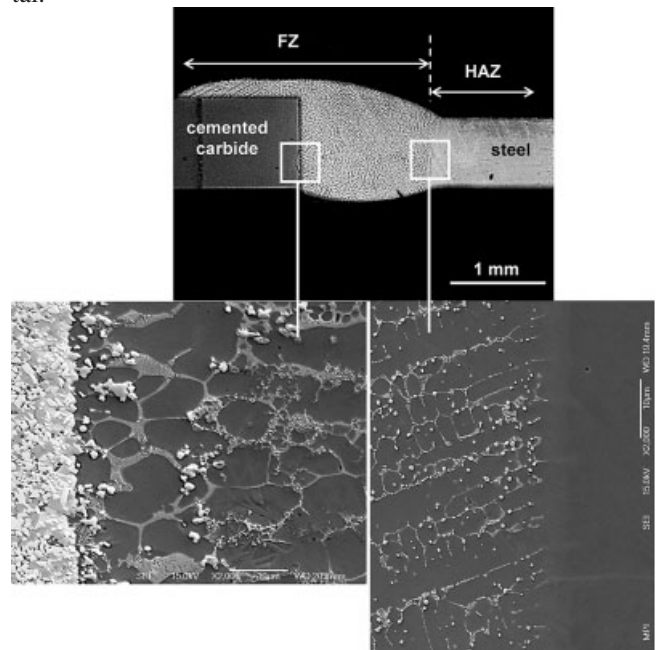

Figure 2. SEM micrographs of the typical bulk microstructure of a) hardmetal and b) cermet.
Bild 2. REM-Aufnahme des Gefüges a) eines Hartmetalls, (b) eines Cermets

Figure 3. Micrograph of a cemented carbide/steel joint. The typical microstructure developed at the interface between the cemented carbide and the fusion zone (FZ) as well as the interface between the fusion zone and the heat affected zone (HAZ) in the steel are shown at higher magnification.
Bild 3. Mikroskopische Aufnahme der Hartmetall-Stahl Verbindung. REM-Aufnahmen der typischen Gefüge an der Grenzfläche Hartmetall-Schmelzzone (FZ) und die Schmelzzone-Wärmeeinflusszone (HAZ).
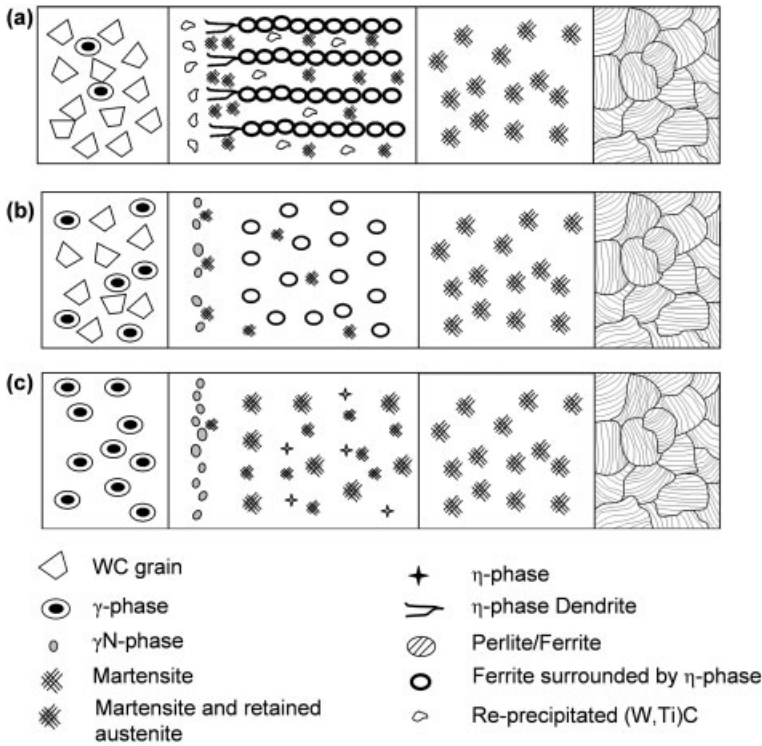
Figure 4. Simplified scheme of the microstructure development in a) hardmetal HM1, b) nitrided hardmetal (HM3), and c) nitrided cermet (HM4) joints, featuring (from left to right) the cemented carbide, the fusion zone consisting of two distinct regions, the heat affected zone in the steel containing mainly martensite, and the parent steel consisting of ferrite-pearlite.

Bild 4. Modelle für Gefügeentwicklung in den Laserstrahlschweißverbindungen: a) Hartmetall-Stahl (HM1), b) nitriertes Hartmetall-Stahl (HM3), c) nitrierter Cermet-Stahl (HM4). Hartmetall/Cermet. Dargestellt sind das Hartmetall bzw. der Cermet die Schmelzzone, die Wärmeeinflusszone (WEZ) des Stahls und der Stahl (jeweils von links nach rechts).

The fusion zone can be divided into two different regions (*Figure 4*). The larger region contains mainly steel with a cell-like distribution of η-phase in a eutectic morphology; it forms a dense and continuous structure and extends from the interface to the steel throughout about 9/10 of the fusion zone.

Figure 5. X-ray diffraction patterns of the fusion zone in the hardmetal/steel and nitrided cermet/steel joints.

Bild 5. Röntgen-Diffraktogramme der Schmelzzone der Hartmetall-Stahl Verbindung und der Verbindung zwischen nitriertem Cermet und Stahl.

Using X-ray diffraction the η-phase could be identified as a mixture of Fe_3W_3C and Fe_6W_6C. X-rays and EDX-analyses in the SEM also revealed the presence of FeW_3C and Fe_7W_6 (*Figure 5, 6 and 7*).

The smaller region of the fusion zone near the interface to the hardmetal contains martensite, WC and mixed carbide particles and also η-phase extending from the WC particles into the network-like η-phase. At the interface between hardmetal and fusion zone intrusions of steel into the hardmetal appear and occasionally large WC and mixed carbide phases are visible.
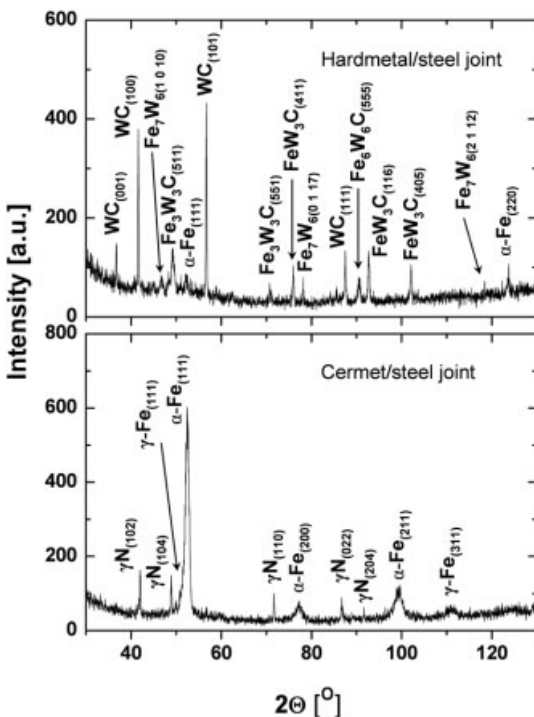
3.2.2 Steel to Nitrided Hardmetal Weld

Similar to the joint between the non-nitrided hardmetal and the steel, the heat affected zone in this joint consists of martensite and extends deeply into the steel.

The diffusion zone again can be divided into two parts (*Figure 8*), the larger part neighbouring the steel containing cells of ferrite, martensite and retained austenite embedded in a very fine network of η-phase. Compared to the weld with the non-nitrided hardmetal the η-phase volume fraction is significantly lower, its size is significantly smaller, and often the network even appears interrupted in the SEM images (*Figure 8c*). X-rays reveal the η-phase also to be a mixture of Fe_3W_3C and Fe_6W_6C.

The part of the fusion zone adjacent to the nitrided hardmetal contains spherical γN-phase particles and slightly thicker η-phase network appear. The amount of γN-phase particles in the fusion zone is distinctly lower than in the nitrided zone of the hardmetal. The interface between the fusion zone and the nitrided hardmetal appears serrated due to steel intrusions into the nitrided layer, η-phase appears in connection to WC particles. A marked heat affected zone is not visible in the hardmetal.
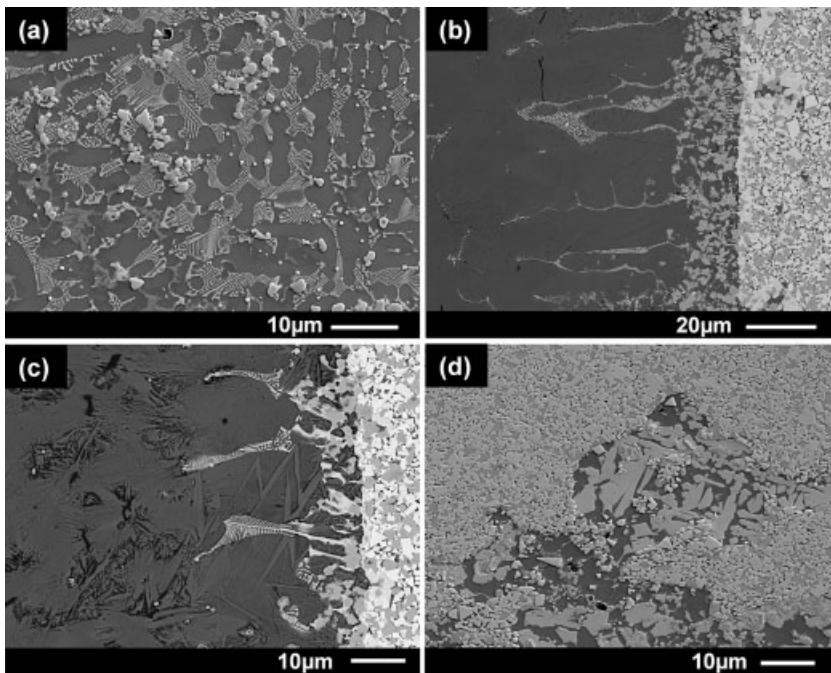
Figure 6. SEM micrographs of the hardmetal/steel welds: a) Microstructure of fusion zone with of *η*-phase, WC and mixed carbide particles. b) Fusion zone at the interface to the hardmetal. c) *η*-phase and martensite. d) Detail of the heat affected zone in the hardmetal showing large mixed carbide grains.

Bild 6. REM-Aufnahmen der Hartmetall-Stahl Verbindung: a) Gefügebild der Schmelzzone mit *η*-Phase, WC und Mischkarbiden. b) Grenzfläche zwischen Schmelzzone und Hartmetall c) *η*-Phase und Martensit d) grobe Mischkarbide in der WEZ des Hartmetalls.
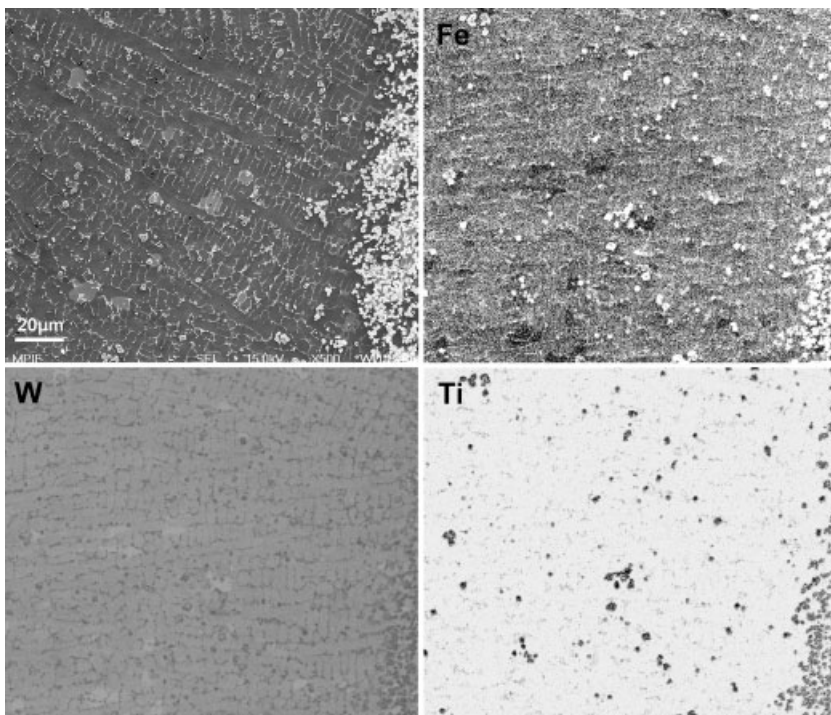

Figure 7. SEM/EDX element maps taken of the fusion zone in the welded joint produced with the hardmetal.

Bild 7. REM-EDX Elementverteilung in der Schmelzzone der Hartmetall-Stahl Verbindung.

3.2.3 Steel to Nitrided Cermet Weld

The heat affected zone of the steel in the cermet/steel joint again contains martensite. The fusion zone consists mainly of martensite containing a small amount of retained austenite. SEM images (*Figure 9*) reveal a very small amount of η-phase, which is not sufficient to build a network but is visible only at some of the grain boundaries of the former austenite grains. In contrast to the steel/hardmetal joints no η-phase concentrations appear at the interface between cemented carbide and fusion zone.

At the cermet side of the fusion zone again steel intrusions into the nitrided layer are visible. Further, occasionally η-phase appears in the nitrided layer, in between γN-phase particles.

3.3 Microhardness

The microhardness of the steel base material is 400 ± 40 $HV_{0.05}$. Microhardness measurements in the hardmetal and the cermet given here represent a composite hardness of hard phases and binder. The average microhardness of the
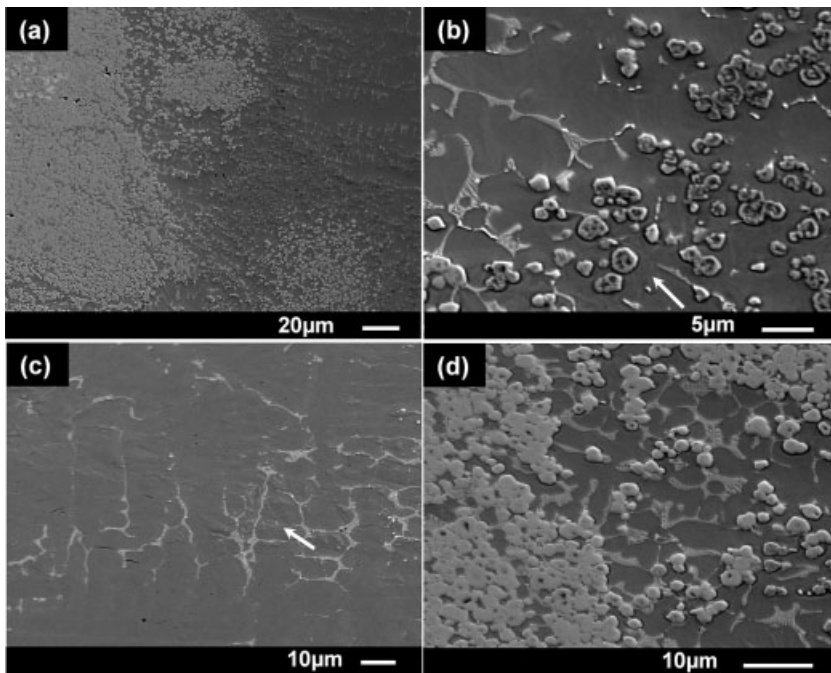
Figure 8. SEM micrographs of the nitrided hardmetal – steel welds: a) Microstructure at the interface between the nitrided layer in the hardmetal and the fusion zone. b) γN-phase grains present in the fusion zone. c) Interrupted network of η-phase. d) Slightly thicker network of η-phase in the fusion zone adjacent to the nitrided layer.

Bild 8. REM-Aufnahmen der Verbindung zwischen nitriertem Hartmetall und Stahl a) Gefüge an der Grenzfläche zwischen nitriertem Hartmetall und Schmelzzone. b) γN-Phase in der Schmelzzone. c) unterbrochenes η-Phasen-Netzwerk. d) Dickeres η-Phasen-Netzwerk an der Grenzfläche Schmelze-nitriertes Hartmetall.
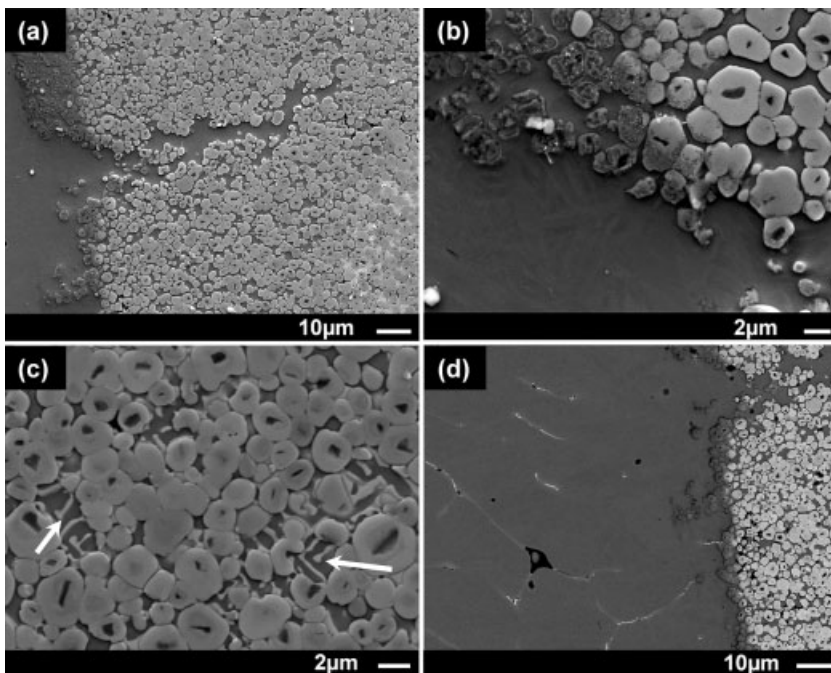

Figure 9. SEM micrographs of cermet-steel welds. a) Interface between fusion zone and cermet HAZ. b) Detail of fusion zone close to cermet HAZ. c) Formation of η-phase eutectic inbetween hard phases. d) η-phase in the fusion zone.

Bild 9. REM-Aufnahmen der Cermet-Stahl Verbindung: a) Gefüge an der Grenzfläche Schmelzzone-Wärmeeinflusszone (WEZ) des Cermets. b) Detail der Schmelzzone und WEZ des Cermets c) η-Phase und Eutektikums zwischen den Carbiden d) η-Phase in der Schmelzzone.

as-sintered hardmetal is 1450 ± 30 HV$_{0.05}$, the average microhardness of the nitrided hardmetal is 1350 ± 50 HV$_{0.05}$. The microhardness of the as-sintered cermet is 1250 ± 50 HV$_{0.05}$; it does not change by the nitridation treatment.

Microhardness measurements were also performed on cross-sections of the welded specimens (*Figure 10*). In case of the nitrided hardmetal and the nitrided cermet microhardness in the fusion zone is almost uniform and in both welds amounts to 700 ± 10 HV$_{0.05}$. In the hardmetal/steel joint in the part of the fusion zone adjacent to the steel also microhardness values of 700 ± 50 HV$_{0.05}$ are reached, the part of the fusion zone adjacent to the hardmetal, however, shows significantly lower hardness values of 520 ± 50 HV$_{0.05}$.

3.4 Residual stresses

The residual stress values given for the hardmetals and the cermet were measured in WC, residual stress values presented for the fusion zone and the steel are phase specific residual stresses of α-iron. Similar residual stress distributions were obtained for all three samples (*Figure 11*). The WC hard phases in the cemented carbide in all three samples are under compressive residual stresses both in welding direction and perpendicular to the welding direction. The steel in the fusion zone and the heat affected zone is generally under tensile residual stresses.

The residual stresses in the WC phase in both heat affected zone and base material in all cemented carbides are usually in
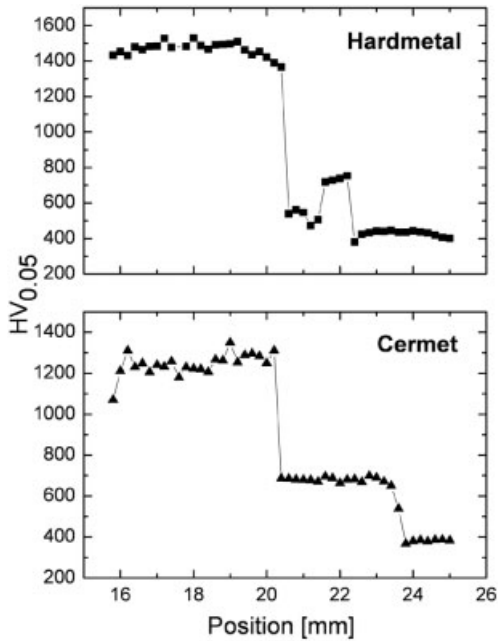
Figure 10. Microhardness profiles across the weld.
Bild 10. Mikrohärte Profile über die Schweißnaht.

the range between -250 MPa and -400 MPa. In the fusion zone of the nitrided hardmetal/steel joint, tensile residual stress values of 200–300 MPa both in welding direction and perpendicular to the welding direction were obtained, whereas in the nitrided cermet, a lower tensile residual stress value of 52 MPa in the welding direction and even compressive residual stresses as low as -460 MPa were measured. In case of the heat affected zone in steel, values of about 400MPa were obtained for the hardmetal joint in welding direction and perpendicular to welding direction, whereas in the cermet joint, tensile stress in the welding direction amounts to 190 MPa, and, in contrast, a value of -300 MPa in the direction perpendicular to the weld-
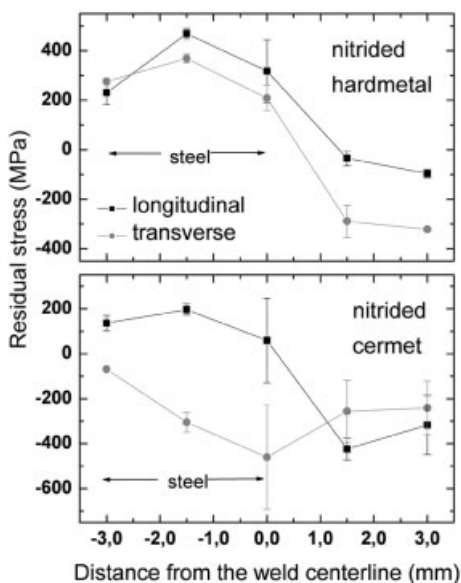

Figure 11. Residual stress profiles of the hardmetal and cermet joints.
Bild 11. Eigenspannungen der Hartmetall-Stahl und Cermet-Stahl Verbindungen.

ing direction was observed. As for the steel base material, residual stresses in the hardmetal are usually tensile in both directions (about 250 MPa), whereas in the cermet they can be as low as 130 MPa in welding direction.

3.5 Bending tests

In bending tests fracture always occurred at the cemented carbide side parallel to the fusion line, in a distance of about 200 to 300 µm to the fusion line. The maximum bending loads sustained are 4950 N±50 N for the nitrided cermet/steel joint, 5050 N±50 N for the nitrided hardmetal/steel joint, 4400 N±50 N for the as-sintered hardmetal steel joint.

4 Discussion

4.1 Phase formation in the fusion zone

Most of the fusion zone consists of steel and the heat affected zone in the steel part is comparatively large. Because of the focussed heat input by the laser the heat affected zone of the steel and the fusion zone cool down rapidly, thus, martensite is formed in the heat affected zone of the steel and in the fusion zone.

The cemented carbides presumably reach temperatures near the (WC-Co)-eutectic. Steel, in its turn, reaches liquidus temperature (T_s: 1362 °C). It then reacts with the eutectic WC-Co and penetrates the cemented carbide, causing decomposition of WC-Co and thus, W and C transport into the fusion zone is established. During cooling W, Fe, and C form a eutectic-containing η-phase mainly at the austenite grain boundaries, thus building a network-like structure. In addition, within the austenite grains (which later transform into martensite) a small amount of WC and mixed carbides precipitate.

The joint with the nitrided hardmetal contained a significantly lower amount of η-phase than the joint with the as-sintered hardmetal. This indicates that the γN-phase hinders the diffusion of W and probably also of C into the melt. Also in case of the nitrided cermet, the γN-phase appears to be an effective barrier for W diffusion into the fusion zone. The barrier function of the γN-phase in combination with the inherently smaller amount of WC in the cermet almost suppresses η-phase formation in the fusion zone. Because C diffuses from the cermet into the fusion and since it is not taken up by η-phase, the steel in the fusion zone of the steel/nitrided cermet weld becomes enriched in C. Martensite start and finish temperatures thus decrease, leading to a microstructure composed of martensite and retained austenite after cooling.

4.2 Joint integrity and origin of residual stresses

If cooling is not controlled, the laser welding process yields strong temperature gradients. Cooling of the weld pool produces shrinkage and thus, inhomogeneous plastic deformation. As a result, in welds often high residual stresses build up – the lower the degree of distortion of the constrained joint, the higher residual stresses are usually found [18].

Residual stress formation in the steel/cemented carbide joints is governed by shrinkage and phase transformation. If similar base materials are welded, cooling usually results in tensile residual stresses in the fusion zone and the heat af-

fected zone balanced by compressive residual stresses in the base material. Martensite formation during cooling, however, increases the volume of the fusion zone and part of the heat affected zone. Thus, martensite transformation in joints of similar steels usually decreases the tensile residual stresses or even produces compressive residual stresses in the fusion zone. In case of the steel/cemented carbide welds, the differences in the heat conductivity and the thermal expansion of the steel and the cemented carbide additionally influence the residual stress state of the weld. Due to the strong mismatch in thermal expansion, cooling can be supposed to introduce compressive residual stresses into the cemented carbide and balancing tensile residual stresses into the steel. The experimental results yielding phase-specific tensile residual stresses in the martensite in the fusion zone and the heat affected zone of the steel indicate a predominance of the strain introduced by the thermal expansion mismatch over the strain generated by the martensitic phase transformation. The experiments also showed that in all joints investigated the WC hard phases in the hardmetal contained phase-specific compressive residual stresses. These phase-specific compressive residual stresses must be understood as a superposition of the welding residual stresses and the micro residual stresses already present in these composite materials. The average values of the micro residual stresses in as-sintered cemented carbides have several times been shown to be compressive in the hard phases and tensile in the metal binder phase [19–21].

The three-step laser welding process presumably reduces residual stress magnitude due to decreasing temperature gradients during welding by pre-heating and controlling the cooling rate during post heat treatment.

4.3 Mechanical properties

The joints produced by laser beam welding have bending strength values comparable to those typically observed in conventional brazed cemented carbide-steel joints [4]. Although some η-phase is present in the welds, it does not form a dense layer near the interface, which has been found to be the main source for a decrease in joint strength of steel-cemented carbide joints e.g. by [7]. The nitridation treatment appears to improve joint bending strength. This presumably can be related to the lower amount of η-phase in joints with nitrided cemented carbides.

5 Conclusions

Laser beam welding allows the successful joining of steel to cemented carbides without filler. By combining welding with a pre-heating and post heat treatment in three-step welding process temperature gradients could be controlled resulting in lower residual stress maximum values and crack-free, non-porous joints. For ensuring joint integrity the cemented carbide part and the steel part should be of equal thickness and the thickness of the joint should not exceed 1.5 mm. A nitridation of the cemented carbides significantly reduces the amount of brittle η-phase formed in the fusion zone and increases joint bending strength. The mechanical strength of joints with nitrided hardmetals and nitrided cermets is comparable to joints produced by conventional brazing processes. In comparison to brazing, the three-step laser beam welding process has the advantages of being faster, more precise and sparing the filler material.

7 References

1. P. Ettmayer, *Annu. Rev. Mater. Sci.* **1989**, *19*, 145.
2. H.E. Exner, *Int. Met. Rev.* **1979**, *243*, 149.
3. K.J.A. Brookes, Handbook of Hardmetals and Hard Materials, 8 Edition, Metal Powder Industry Federation, **1997**.
4. L. Martens, W. Tillmann, E. Lugscheider, G. Ziegler, *J. Mater. Proc. Technol.* **1996**, *58,* 13.
5. H. Zhang, J.Senkara, Resistance Welding: Fundamentals and Applications, CRC Publications, **2005**.
6. G.S. Upadhyaya, Cemented Tungsten Carbides: Production, Properties, and Testing, Noyes Publications, Westwood, New Jersey **1998**.
7. H. Stroißnigg, W. Waldhauser, R. Ebner, *BHM* **2003**, *148, Heft 7, 288*.
8. S. Sandig, P. Wiesber, M. Greitmann, G. Deutschmann, Laser Welding of Hard Metal Components onto Steel, DVS Berichte 163, Germany **1994**.
9. S. Sandig, P. Wiesner, M. Greitmann, G. Deutschmann, Technological Aspects of Laser Joining of Steel and Hard Metal Components, Proceedings ICALEO **1995**.
10. A. Costa, L. Quintino, Hard Metals Irradiation by a (cw) CO_2 Laser Beam, Joining of Materials, **2001**.
11. A.P. Costa, L. Quintino, M. Greitmann, J. Mater. Proc. Technol. **2003**, *141*, 163.
12. N. Franz, G. Liedl, US Patent 6 310 314, **2001**.
13. P. Müller, E. Macherauch, *Z. ang. Phys.* **1961**, *13*, 305.
14. J. Zackrisson, U. Rolander, B. Jansson, H.-O. André, Acta Mater. **2000**, *48*, 4281.
15. C.F. Barbatti, F. Sket, J. Garcia, A. Pyzalla, *Surf. Coat. Technol.* **2006**, *201*, 3314.
16. P. Lindhal, P. Gustafson, U. Rolander, L. Stals, H.-O. André, *Int. J. Refract. Met. Hard Mater.* **1999**, *17*, 411.
17. H. Holleck, Binäre und ternäre Carbide und Nitridsysteme der Übergangsmetalle, Gebrüder Borntraeger, Berlin-Stuttgart, **1984**.
18. Th. Nitschke-Pagel, H. Wohlfahrt, The generation of residual stresses due to joining processes, In : Residual Stresses: Measurement, Calculation, Evaluation (Eds. V. Hauk, H. Hougardy and E. Macherauch), DGM Verlag, Oberursel, Germany, **1991**.
19. D. Mari, A. D. Krawitz, J.W. Richardson, W. Benoit, Mater. Sci. Eng. A **1996**, *209*, 197.
20. A. Pyzalla, C. Genzel, W. Reimers, *Mater. Sci. Eng. A* **1996,** *212*, 130.
21. A. Pyzalla, W. Reimers, *Physica B* **1997**, *234–236*, 974.

Correspondence author: Dr. Carla Barbatti,
Max-Planck-Institut für Eisenforschung GmbH,
40237 Düsseldorf,
E-Mail: c. barbatti@mpie.de